

Engineering Surface Architectures for Improved Durability in III–V Photocathodes

Micha Ben-Naim, Chase W. Aldridge, Myles A. Steiner, Reuben J. Britto, Adam C. Nielander, Laurie A. King, Todd G. Deutsch, James L. Young,* and Thomas F. Jaramillo*



Cite This: <https://doi.org/10.1021/acsami.1c18938>



Read Online

ACCESS |



Metrics & More



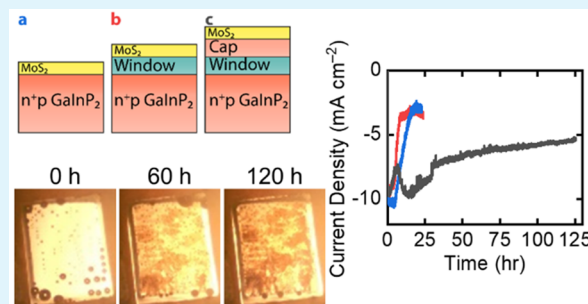
Article Recommendations



Supporting Information

ABSTRACT: GaInP₂ has shown promise as the wide bandgap top junction in tandem absorber photoelectrochemical (PEC) water splitting devices. Among previously reported dual-junction PEC devices with a GaInP₂ top cell, those with the highest performance incorporate an AlInP₂ window layer (WL) to reduce surface recombination and a thin GaInP₂ capping layer (CL) to protect the WL from corrosion in electrolytes. However, the stability of these III–V systems is limited, and durability continues to be a major challenge broadly in the field of PEC water splitting. This work provides a systematic investigation into the durability of GaInP₂ systems, examining the impacts of the window layer and capping layer among single junction pn-GaInP₂ photocathodes coated with an MoS₂ catalytic and protective layer. The photocathode with both a CL and WL demonstrates the highest PEC performance and longest lifetime, producing a significant current for >125 h. In situ optical imaging and post-test characterization illustrate the progression of macroscopic degradation and chemical state. The surface architecture combining an MoS₂ catalyst, CL, and WL can be translated to dual-junction PEC devices with GaInP₂ or other III–V top junctions to enable more efficient and stable PEC systems.

KEYWORDS: photoelectrochemistry, water splitting, III–V, GaInP₂, protective layers



INTRODUCTION

Photoelectrochemical (PEC) water splitting is envisioned to be a direct solar-driven technology to split water into hydrogen and oxygen in a potentially sustainable manner.^{1,2} PEC devices designed for water splitting integrate semiconductor absorbers with catalyst materials to drive the oxygen evolution reaction (OER) and hydrogen evolution reaction (HER).³ Tandem absorber configurations have received considerable attention as two junctions can absorb a wide range of the solar spectrum while producing sufficient voltage to split water, bridging the thermodynamic potential (1.23 V) and kinetic overpotentials for the OER and HER (~0.3–0.5 V total for state-of-the-art precious metal catalysts).^{4–6} To date, III–V semiconductor-based systems have achieved the highest efficiencies for unassisted PEC water splitting.³ Lattice-matched GaInP₂/GaAs tandems have demonstrated solar to hydrogen efficiencies (η_{STH}) surpassing 10%.^{7–9} Recent reports on lattice mismatched GaInP₂/Ga_{1-x}In_xAs tandem devices grown with a metamorphic buffer have shown η_{STH} exceeding 16%¹⁰ and 19%.¹¹ However, the stability of these devices remains limited, with lifetimes in the range of 1 h¹¹ to 100 h.⁸ The United States Department of Energy (DOE) long-term technology goal for photoelectrode lifetime is 10 years (or >17 000 h under illumination assuming a 20% capacity factor),^{12,13} so large-scale deployment of PEC water splitting

will require the development of PEC devices with vastly improved durability.

In devices incorporating a Ga_{0.51}In_{0.49}P (hereafter GaInP₂) top cell (1.81 eV bandgap), the addition of a thin Al_{0.53}In_{0.47}P (hereafter AlInP₂) window layer (WL) has been shown to passivate the GaInP₂ surface and decrease surface recombination compared to the pn-GaInP₂ junction, increasing the current density and voltage much like in traditional photovoltaic (PV) devices.^{9,10,14} However, AlInP₂ can corrode in acidic environments,¹⁵ so a thin semiconductor capping layer (CL) is often added on top of the WL to protect the AlInP₂ window from dissolution.^{10,16} The CL material should be stable in electrolyte, lattice-matched to the underlying device, and relatively transparent by having a wide bandgap and/or being thin enough to minimize parasitic light absorption. In previous studies, the CL has been composed of GaInP₂, the same material as the absorber, so it can parasitically absorb light, decreasing current density. However, other III–V

Special Issue: Materials and Interfaces for Energy Storage and Conversion

Received: September 30, 2021

Accepted: December 21, 2021

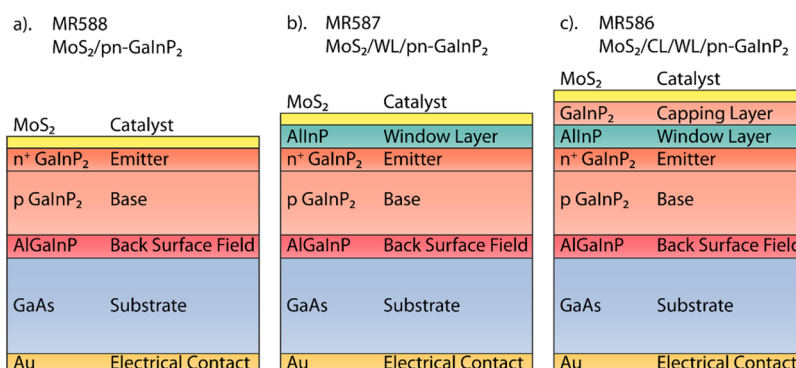


Figure 1. Device schematics for GaInP₂ photocathode architectures tested in this work, not drawn to scale: (a) MoS₂/GaInP₂, (b) MoS₂/WL/GaInP₂, (c) MoS₂/CL/WL/pn-GaInP₂. All photocathodes are epitaxially grown on a GaAs substrate and have an AlGaInP back surface field layer, Au back contact, and MoS₂ catalyst on the surface. NREL sample numbers are MR588, MR587, and MR586 for a–c, respectively.

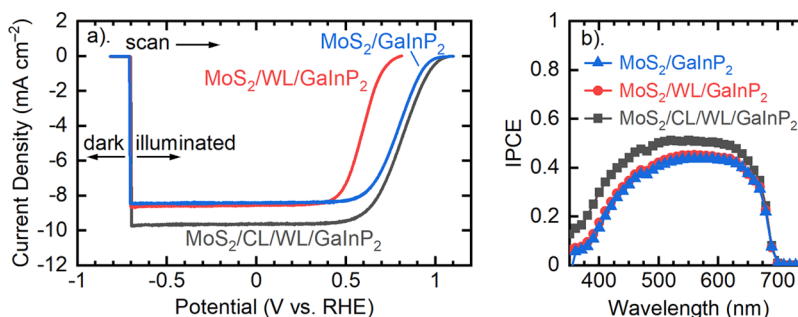


Figure 2. Photoelectrochemical characterization. (a) LSVs under 1-sun illumination for the three photocathodes. (b) IPCE across the absorbable range for each photocathode at 0.08 V vs RHE. The MoS₂/CL/WL/GaInP₂ has the most positive onset potential and highest J_{sat} .

materials meeting the aforementioned material constraints can be used as a CL.¹⁶ This design motif pairing a WL and CL with a pn-GaInP₂ top junction is common to several of the highest efficiency tandem PEC systems to date,^{9,10} motivating efforts to understand how the CL and WL impact the stability of the GaInP₂ top junction.

PEC devices also require an effective electrocatalyst material to achieve the highest efficiency, and the ideal material would both act as a catalyst for the reaction of interest and inhibit corrosion, resulting in photoelectrodes with improved efficiency and durability compared to the bare semiconductor.^{8,12,17,18} MoS₂ is an effective and stable HER catalyst that can also function as a protection layer by isolating the semiconductor from contact with the electrolyte.^{12,19–22} Prior studies have compared MoS₂-based coatings with nanoparticulate catalysts that expose the semiconductor to the electrolyte, and the MoS₂ coatings led to improved device durability, demonstrating that MoS₂-based layers impart corrosion protection.^{12,21,22} Prior work pairing MoS₂ with a variety of semiconductor materials, including silicon,^{23–25} GaInP₂,^{21,22,26,27} and GaInAsP/GaAs¹² has demonstrated effective photocathodes. However, evaluating the effectiveness of protecting layer schemes depends not only on the chemical characteristics of the protective materials themselves but also on the interaction of the protective layers with the underlying materials in the PEC device.

In this work, we pair MoS₂ catalytic protection layers with GaInP₂ photocathodes to investigate the impacts of a WL and CL on photocathode stability. pn-GaInP₂ photocathodes incorporating no WL, a WL, and a WL and CL are fabricated and coated with an MoS₂ catalyst, and all exhibit high PEC activity. *In situ* optical microscopy and X-ray photoelectron

spectroscopy (XPS) were harnessed to characterize the degradation pathways of the photocathodes. We show that, when coupled with an MoS₂ catalyst, the CL can stabilize the WL and lead to photocathode lifetimes >120 h.

RESULTS AND DISCUSSION

Photocathode Design and Fabrication. Three GaInP₂ photocathode architectures were grown by metalorganic vapor phase epitaxy (MOVPE) on GaAs substrates (Figure 1). Detailed photocathode fabrication procedures can be found in the [Experimental Methods](#). The simplest photocathode architecture, buried junction pn-GaInP₂ with an MoS₂ catalyst (referred to as MoS₂/GaInP₂), matches the designs in prior reports and serves as a reference to which the PEC performance of the other two photocathodes is compared (Figure 1a).²² In the second photocathode architecture, a 20 nm AllnP window layer (WL) intervenes between the MoS₂ and GaInP₂ layers (MoS₂/WL/GaInP₂) (Figure 1b). The third photocathode architecture includes both a 20 nm WL and a 15 nm GaInP₂ capping layer (CL) (MoS₂/CL/WL/GaInP₂) (Figure 1c). MoS₂ was deposited on each photocathode, serving as an HER catalyst and protecting layer, using a previously developed process consisting of sputtering a ~3.6 nm Mo metal film followed by a partial thermal sulfidization treatment.^{12,21,22,24} XPS measurements indicate that the MoS₂ coating contains MoS₂, metallic Mo, and MoO_x character (Figures S1 and S2),²⁸ which matches the structure of prior reports using this MoS₂ coating procedure.^{21,23,24} Prior reports depositing MoS₂ onto III–Vs using the same deposition process showed a total layer thickness of ~5 nm, so the MoS₂ coating is expected to have a similar thickness in this work.

Photoelectrochemical Characterization. The PEC performance of the photocathodes was evaluated using established protocols (see [Experimental Methods](#)),^{10,29} with measurements conducted in a two-compartment cell under 1-sun nominally AM1.5G illumination calibrated with a 1.81 eV bandgap GaInP₂ reference diode. Linear sweep voltammograms (LSVs) were measured in a three-electrode configuration using an IrO_x counter electrode and a Hg/Hg₂SO₄ reference electrode to determine the onset potential (E_{onset}) and light-limited current density (J_{sat}) ([Figure 2a](#) and [Table 1](#)).

Table 1. PEC Performance Metrics

photocathode architecture	E_{onset} (V vs RHE)	J_{sat} (mA cm ⁻²)	J_{IPCE} (mA cm ⁻²)	total charge passed (C cm ⁻²)
MoS ₂ /GaInP ₂	0.93 ± 0.01	-8.5 ± 0.2	-7.0	420
MoS ₂ /WL/GaInP ₂	0.70 ± 0.002	-8.6 ± 0.2	-7.2	510
MoS ₂ /CL/WL/GaInP ₂	0.92 ± 0.04	-9.6 ± 0.04	-8.6	3090

Scans were measured from more negative to more positive potential and were stopped when the current density reached ~0 mA cm⁻². Here, E_{onset} is taken as the potential where the photocurrent density reaches -1 mA cm⁻².¹² LSVs were measured for three or four replicate samples for each photocathode design ([Figure S3](#)). Performance metrics (E_{onset} and J_{sat}) for all replicates are detailed in [Table S2](#), and the averages are shown in [Table 1](#) and described in what follows. The MoS₂/GaInP₂ photocathodes demonstrated an average onset potential of 0.93 ± 0.01 V vs RHE ([Figure 2a](#), [Figure S3a](#)), consistent with prior reports.²² The MoS₂/WL/GaInP₂ resulted in an onset potential of 0.70 ± 0.002 V vs RHE, a decrease of 0.23 V compared to the reference MoS₂/GaInP₂ ([Table 1](#)), with an explanation for this performance decrease found below. The MoS₂/CL/WL/GaInP₂ exhibited an onset potential similar to that of the MoS₂/GaInP₂ devices, 0.92 ± 0.04 V vs RHE, so these architectures have a similar photovoltage (or alternately similar voltage losses). J_{sat} is another important figure of merit when evaluating PEC device performance as it directly influences the attainable η_{STH} . As the photocurrent density is constant with potential in the saturation region, J_{sat} is taken as the average photocurrent density around 0 V vs RHE. The WL acts as a surface passivation layer by reducing nonradiative recombination at the surface of the pn-GaInP,¹⁰ but MoS₂/WL/GaInP₂ provides a photocurrent density similar to that of MoS₂/GaInP₂, generating -8.6 ± 0.2 mA cm⁻² and -8.5 ± 0.2 mA cm⁻², respectively. In contrast, the MoS₂/CL/WL/GaInP₂ generates -9.6 ± 0.04 mA cm⁻², an increase of -1.1 mA cm⁻², or 13%, compared to MoS₂/GaInP₂, suggesting that the CL is required to achieve the full photocurrent benefits provided by the WL. This increased photocurrent density also indicates that the surface passivation by the WL increases the current more than the parasitic light absorption in the CL decreases current. The J - V behavior of each device architecture was also probed in the absence of illumination at the beginning (-0.75 to -0.6 V vs RHE) of the positive-going LSV scans ([Figure 2a](#)). The minimal dark current indicates that all observed current is photocurrent (i.e., generated from light absorption).

Incident photon-to-current efficiency (IPCE) was then measured to probe the spectral response of the photocathodes

([Figure 2b](#)). The spectral response is 0 for wavelengths higher than 690 nm, consistent with the bandgap of GaInP₂, 1.81 eV. The maximum IPCE value is ~0.45–0.51, well below the reflection limit of 0.75 for III–V/electrolyte optical interfaces.³⁰ The MoS₂ coating has some Mo metal that has been shown in previous reports to attenuate ~30–40% of visible light, likely leading to the lower measured IPCE in these photocathodes.^{21,24} Further optical characterization could be used to understand how the MoS₂, WL, and CL impact light absorption and reflection.²⁴ Integrating the IPCE response over the reference solar spectrum gives the expected maximum current density under standard AM1.5G illumination (as opposed to the measured current density under the particular laboratory lamp), with values found in [Table 1](#).^{30,31} Consistent with the measured current density ([Figure 2a](#)), MoS₂/CL/WL/GaInP₂ has the highest J_{IPCE} , 22% higher with respect to MoS₂/GaInP₂ ([Table 1](#)). MoS₂/WL/GaInP₂ has J_{IPCE} only 3% higher than that of MoS₂/GaInP₂. Overall, the LSV and IPCE results demonstrate that the addition of a CL and WL to a GaInP₂ photocathode yields improved PEC activity in terms of both photocurrent density and onset potential.

Durability Analysis. To investigate the durability of the photocathodes, we measured chronoamperometry (CA) under nominally AM1.5G 1-sun illumination at a potential of 0.18 V vs RHE ([Figure 3](#)). This potential was chosen as it is a slightly

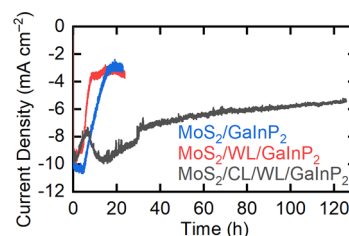


Figure 3. Chronoamperometry measurements for the three photocathode architectures at 0.18 V vs RHE. The MoS₂/CL/WL/GaInP₂ photocathode exhibited the longest lifetime, producing a significant current for >120 h.

lower potential than the onset of saturation photocurrent density, which represents an ideal operating condition in a tandem device and avoids masking degradation with extra bias.^{10,22,32} *In situ* optical microscopy was collected during the durability measurements to monitor macroscopic degradation ([Figure 4](#), [Movies S1](#), [S2](#), [S3](#)). Hydrogen bubbles are visible on all three photocathodes, particularly at the beginning of each durability test ([Figure 4](#)). The MoS₂/GaInP₂ photocathode demonstrated a stable current density for the first 5 h ([Figure 3](#)). During the initial 3.5 h, there were no changes to the photoelectrode visible in the optical microscopy data ([Figure 4a](#), [Movie S1](#)). Over the next 12 h, the photoelectrode slowly degraded, as evidenced by the areas of dark contrast in the optical microscopy growing to encompass nearly the entire electrode surface. This period of degradation corresponds with a steady decrease in the magnitude of the current density from -10 mA cm⁻² to -3 mA cm⁻² from 5 to 15 h of testing ([Figure 3](#)). The current density over the last 8 h of testing was steady at -3 mA cm⁻² before the test was terminated at 23 h. During this period, the rate of macroscopic degradation was slower than during the middle of the test. The MoS₂/WL/GaInP₂ photocathode was less stable than MoS₂/GaInP₂, with the current density decreasing between 4.4 and 8.5 h of testing

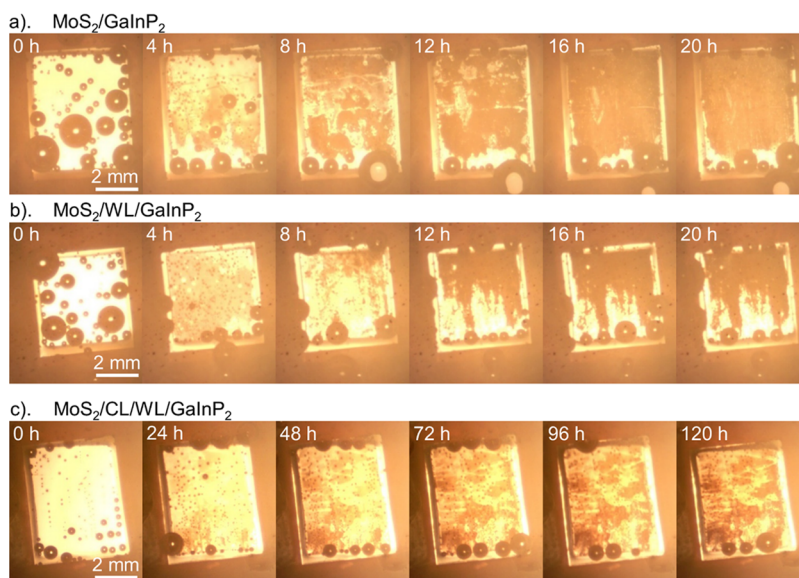


Figure 4. Optical microscope images of photocathodes during stability testing. (a) MoS₂/GaInP₂, (b) MoS₂/WL/GaInP₂, (c) MoS₂/CL/WL/GaInP₂. Degradation is shown by darker contrast in the images. Hydrogen bubble nucleation is also visible in the circular features, and the epoxy appears as a thin border around the edge of the brighter, rectangular semiconductor material. Full time lapse movies can be seen in the Supporting Information (Movies S1, S2, S3).

and stabilizing at around -3 mA cm^{-2} until the CA was aborted at 24 h. Similar to MoS₂/GaInP₂, the MoS₂/WL/GaInP₂ photocathode initially displayed a slow rate of macroscopic corrosion that accelerated at the same time as the current density decreased (Figure 4b, Movie S2). At the end of the durability test when the current density was roughly constant, the sample surface remained unchanged from a macroscopic view, suggesting minimal degradation during this time.

MoS₂/CL/WL/GaInP₂ demonstrated the most stable current–time behavior of the three photocathodes. After an initial decrease in current density over the first 6.5 h, the current density returned to the starting value of $\sim -9.7 \text{ mA cm}^{-2}$ at 14 h. The photoelectrode experienced minor macroscopic changes during the initial period of decreasing current density, with small areas of discoloration around 3–4 h of testing (Figure S4, Movie S3). However, this macroscopic degradation disappeared around 5 h, and there were minimal macroscopic features during the period of increasing current density from 6.5–14 h. For the remainder of the CA, the current then slowly decreased, ending at -5.3 mA cm^{-2} after 125 h of testing. A replicate MoS₂/CL/WL/GaInP₂ device also exhibited an initial decrease and recovery in current density followed by a slow decrease in current density (Figure S5). This dynamic current–time behavior motivates future studies probing the material structure by techniques such as SEM or XPS as a function of testing time. The charge passed by the MoS₂/CL/WL/GaInP₂ photocathode was >6 times greater than either of the other photocathode architectures (Table 1). The macroscopic degradation was also the slowest and least severe for MoS₂/CL/WL/GaInP₂ compared to the other photocathode designs. The optical images over the last 2 days of the test appear unchanged, so large-scale corrosion is likely slow during this time. The degradation features were also spatially heterogeneous; the left edge of the photoelectrode became more damaged than the center or right side. The observed PEC stability and slow rate of macroscopic corrosion indicate that the CL is effective and necessary to stabilize the

WL and that including both a CL and WL on the surface of GaInP₂ led to improved PEC durability. From prior work on MoS₂-protected III–V photocathodes, both defects and edge effects can contribute to macroscopic degradation, and both are likely contributing to degradation for these GaInP₂ photocathodes.¹² For all samples, the bubble nucleation sites become more concentrated around the edges and less prevalent in the center for each sample over the first several hours, which could be associated with degradation around the edges and decreasing current over time. Because all photocathode samples do exhibit macroscopic changes, it is possible that some of the measured photocurrent is due to photo-corrosion of the semiconductor layers rather than HER current as intended. However, the amount of charge passed is significantly larger than the amount of current that would be required to dissolve the entire GaInP₂ layer, so only a small fraction of the current could be due to corrosion (see Supporting Note 1 for more details).³³

After the CA durability tests, XPS characterization was conducted on each photoelectrode to illustrate chemical changes and probe the degradation mechanisms (Figure 5). The X-ray beam was aimed at the center of each electrode, to within the resolution of the digital camera in the XPS tool. Both the MoS₂/GaInP₂ and MoS₂/CL/WL/GaInP₂ photocathodes show Mo in the near-surface region after the 23 and 125 h CA measurements, respectively (Figure 5a). Similarly, both photocathodes have a S 2p peak at $\sim 162 \text{ eV}$, assigned to the S²⁻ state, indicating that there is still MoS₂ left on the surface (Figure 5b).^{23,24} There is also a peak at $\sim 168 \text{ eV}$ for all three photocathodes that is attributed to the oxidized S⁶⁺ state in SO₄²⁻ from residual electrolyte adsorbed on the surface, consistent with prior reports.^{23,24} The XPS spectra for neither MoS₂/GaInP₂ nor MoS₂/CL/WL/GaInP₂ show significant peaks for Ga, In, or P (Figure 5c–e), suggesting that the remaining MoS₂ layer plus adventitious carbon are thick enough to prevent photoelectrons generated in the semiconductors from escaping the sample. In contrast, the MoS₂/WL/GaInP₂ photocathode shows no Mo or S²⁻ by XPS, while

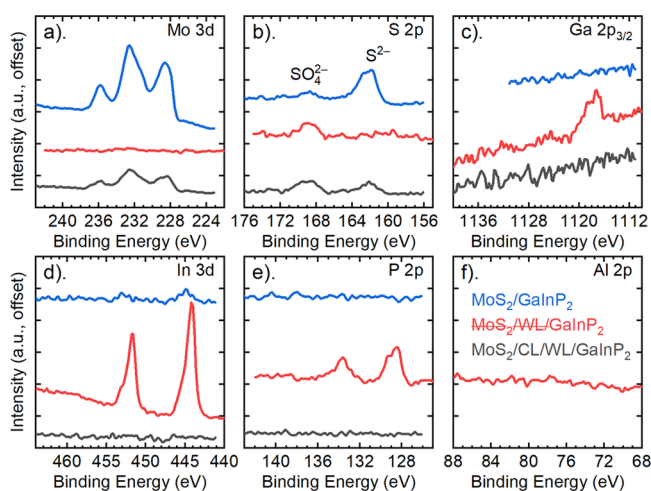


Figure 5. XPS measurements post-test. The following peaks are shown: (a) Mo 3d, (b) S 2p, (c) Ga 2p_{3/2}, (d) In 3d, (e) P 2p, (f) Al 2p. The MoS₂/WL/GaInP₂ photocathode has no MoS₂ or AlInP₂ (WL) on the surface to the detection limits of XPS and is most accurately a bare pn-GaInP₂ surface. Hence, the legend has the MoS₂/WL crossed out.

sulfur in the S⁶⁺ state associated with SO₄²⁻ was detectable. The pre-test XPS spectrum did show significant Mo 3d and S 2p peaks (Figures S1 and S2). Thus, the MoS₂ layer is not present by the end of the durability test. The absence of an Al peak in XPS suggests that the AlInP₂ WL, which is directly beneath the MoS₂ in this photocathode architecture, also dissolved (Figure 5f). Peaks for Ga 2p, In 3d, and P 2p are present, indicating that the top surface for the MoS₂/WL/GaInP₂ after testing is GaInP₂. For comparison, the pre-test XPS spectrum of MoS₂/WL/GaInP₂ had an In 3d peak visible but no Ga 2p or P 2p (Figure S1). While MoS₂ catalyst coatings have demonstrated stability in acid,^{22,23} AlInP₂ is known to be unstable in aqueous electrolytes.¹⁰ The heterogeneity and incomplete sulfidation of the MoS₂ coating likely allow the AlInP₂ WL to dissolve completely and rapidly, causing instability in the overlying MoS₂, likely leading to delamination and/or dissolution. Thus, the legend for Figure 5 denotes the MoS₂/WL with a strikethrough to emphasize that the resulting structure is more likely a bare GaInP₂ surface. LSVs measured after the durability tests show a lower light-limited current density and more negative onset potential than in the initial LSVs in Figure 2a (Figure S6). This loss in PEC performance is consistent with the observed decrease in photocurrent during the CA measurement and material degradation probed by optical microscopy and XPS.

This post-test characterization helps rationalize the observed trends in photocurrent density and onset potential. The MoS₂/WL/GaInP₂ photocathode had the most negative onset potential of the three device architectures. We speculate that even during the initial LSVs, the surface layers MoS₂/WL/GaInP₂ photocathode had begun to degrade. Pinholes or other defects in the MoS₂ could allow the electrolyte to dissolve the AlInP₂ underneath the MoS₂, and the instability of the AlInP₂ WL would lead to rapid dissolution. If the underlying WL dissolves, then the MoS₂ could degrade or delaminate. Incomplete MoS₂ coverage would mean that some GaInP₂ would have to catalyze HER instead of MoS₂, leading to higher overpotential required to drive HER and thus a more negative onset potential. The WL is also expected to increase the light-

limited current density by reducing surface recombination.¹⁴ However, the MoS₂/WL/GaInP₂ photocathode has a current density similar to MoS₂/GaInP₂ and a lower current density than MoS₂/CL/WL/GaInP₂, which is consistent with degradation of the WL before the LSV and IPCE. While the MoS₂ layer has been shown to attenuate light (and lead to lower current density), the worse charge carrier extraction likely counteracts the increased light absorption from a partially (or even fully) degraded MoS₂/WL/GaInP₂ surface compared to MoS₂/GaInP₂.^{22,24} In addition, the incorporation of the AlInP₂ WL reduced device stability even with the presence of a MoS₂ protective layer, which indicates a reduced tolerance to defects in the protective layer and/or reduced adhesion of MoS₂ to AlInP₂ with respect to GaInP₂. On the other hand, the addition of the CL to the MoS₂/CL/WL/GaInP₂ photocathode returned the desired device stability and attained the improved photovoltaic performance expected from the WL. The promising performance and durability motivate the use of a MoS₂/CL/WL/GaInP₂ architecture in future tandem absorber designs incorporating GaInP₂ and other III–V semiconductor top cells.

While this study uses GaInP₂ as a CL, in principle other lattice-matched III–V materials can be used as CLs subject to the material constraints of stability, transparency, and optimal band alignment with respect to the bands of the absorber material and redox reaction potentials. For example, a thin GaInAsP layer (bandgap ~1.7–1.8 eV) could act as a CL with GaInP₂ photocathodes.^{12,34} Using a more intrinsically stable CL than GaInP₂ could lead to improved device durability compared to those demonstrated in this work. However, as seen in this work, evaluating CL effectiveness for photoelectrodes is dependent on interactions with the catalyst, WL, and any other layers in the PEC system.

CONCLUSIONS

In summary, the surface architecture of GaInP₂ photocathodes was investigated to determine the impact of an AlInP₂ WL and GaInP₂ CL on photocathode durability when used in combination with an MoS₂ catalyst. Devices with a WL only and both a WL and a CL were fabricated and compared to a baseline pn-GaInP₂ photocathode in terms of the PEC performance and stability. The MoS₂/CL/WL/GaInP₂ photocathode demonstrated both the best activity and durability, while MoS₂/WL/GaInP₂ had a lower onset potential and the shortest lifetime. *In situ* optical characterization illustrated that macroscopic degradation and loss in photocurrent occurred concomitantly. From post-test XPS and the PEC results, the WL dissolves and likely removes all MoS₂ during this dissolution, leaving a bare pn-GaInP₂ photocathode. The MoS₂/CL surface, however, can adequately protect the WL from corrosion in electrolyte. This study also highlights the importance of evaluating the efficacy of photoelectrochemical protective layers as a function of the entire device architecture. These findings help rationalize the CL/WL/GaInP₂ architecture used in existing devices, and translating the MoS₂/CL/WL surface to other top cell materials could help realize tandem absorber devices with higher efficiency and improved stability.

EXPERIMENTAL METHODS

Photocathode Fabrication. Samples were grown at NREL by atmospheric pressure metalorganic vapor phase epitaxy (MOVPE) on a custom-built vertical reactor. Source materials included trimethylgallium, triethylgallium, trimethylindium, and trimethylaluminum for

the group-III elements; arsine and phosphine for the group-V elements; and diethylzinc, carbon tetrachloride, disilane, and dilute hydrogen selenide for the dopants.

The samples were grown on single-side polished, zinc-doped (001) GaAs substrates, miscut 4° toward the $\langle 111 \rangle$ B direction. The wafers were cleaved into 20 mm \times 30 mm pieces and etched for two minutes in $\text{NH}_4\text{OH}/\text{H}_2\text{O}_2/\text{H}_2\text{O}$ (2:1:10 by volume) to remove any cleave dust. The samples were then loaded onto a graphite susceptor in the reactor and inductively heated to 700 $^\circ\text{C}$ under an arsine overpressure, in a purified hydrogen carrier gas of 6 L min^{-1} . After deoxidization at 700 $^\circ\text{C}$ for 10 min, a GaAs seed layer was grown, followed by 500 nm of $\text{Al}_{0.3}\text{Ga}_{0.7}\text{As}$ and then the full semiconductor structure, all at 700 $^\circ\text{C}$. The reactor was then cooled to 650 $^\circ\text{C}$, and a GaAs front contact layer was grown, to enable PV test structures to be fabricated, and then the reactor was cooled under an arsine overpressure. The active layers were grown at $\sim 6.4 \mu\text{m h}^{-1}$. For these cells, the GaInP_2 base layers were doped with zinc, and the emitter, WL, and CL were all doped with selenium.

Following growth, a gold back contact was electroplated to the substrate side, after the substrate was cleaned in $\text{NH}_4\text{OH}/\text{H}_2\text{O}_2/\text{H}_2\text{O}$ (2:1:10 by volume). For PEC devices, the GaAs front contact layer was etched away in $\text{NH}_4\text{OH}/\text{H}_2\text{O}_2/\text{H}_2\text{O}$ (2:1:10 by volume).

The MoS_2 catalyst coating was deposited following previously developed methods.^{12,21,24} In brief, the GaAs contact layer deposited on the top surface of all three photocathodes was etched for 60 s in a solution of NH_4OH and H_2O_2 in water in a volume ratio of 2:1:10. Then, a thin metallic Mo film (nominally 3.6 nm) was deposited via DC magnetron sputtering (Kurt J. Lesker) with a power of 200 W for 14 s at a nominal deposition rate of 15 nm min^{-1} . The Mo metal was converted to the MoS_2 catalyst by annealing in a tube furnace (Mellen 1 zone) at 250 $^\circ\text{C}$ for 1 h in a 10% $\text{H}_2\text{S}/90\%$ H_2 atmosphere.

Photoelectrodes were prepared by cleaving the MoS_2 -coated GaInP_2 wafers into rectangular pieces (surface area 0.2–0.3 cm^2). Colloidal silver paste (PELCO 16031) was used to attach and form an electrical contact between a copper tape lead and the gold back contact of the electrode. The copper tape and electrode were mounted on a glass slide for mechanical stability. The copper tape, glass slide, and sides of the photoelectrodes were coated in epoxy (Loctite Hysol 9462). The perimeter of the photoelectrodes was also covered with epoxy, exposing only the front surface of the $\text{MoS}_2/\text{GaInP}_2$ photoelectrode to the electrolyte. The entire area of the photoelectrode (including the portions covered with epoxy) was taken as the photoactive surface area as the translucent epoxy allows photon absorption in the GaInP_2 .³⁰

Photoelectrochemical Characterization. Photoelectrochemical characterization utilized a SP-300 potentiostat (BioLogic) and were conducted in a flat-faced glass cell filled with 0.5 M sulfuric acid (OmniTrace EMD Millipore) electrolyte with 1 mM Triton X-100 surfactant (EMD Millipore). Measurements were conducted in a three-electrode configuration with a $\text{Hg}/\text{Hg}_2\text{SO}_4$ reference electrode (0.5 M H_2SO_4) and an IrO_x -coated Ti mesh counter electrode. The counter electrode was contained in a glass tube with a frit filled with the same electrolyte as the main cell. Isolating the counter electrode has been shown in prior reports to mitigate fouling at the counter electrode from degradation of the surfactant.²⁹ Linear sweep voltammetry (LSV) was measured from a more negative potential to a more positive potential with a scan rate of 20 mV s^{-1} . During initial LSVs, a Xe arc lamp solar simulator (ABET Technologies) was used to illuminate photoelectrodes and was set to nominally AM1.5G 1-sun intensity using a GaInP_2 (1.81 eV) reference diode. The incident photon-to-current efficiency (IPCE) was measured with 10 nm full width at half-maximum (fwhm) resolution in a three-electrode configuration using the PEC device as the working electrode. The $\text{Hg}/\text{Hg}_2\text{SO}_4$ reference electrode (0.5 M H_2SO_4) and Pt counter electrode were the same as those used in the LSV measurements. The electrodes were submerged in a glass cell containing 0.5 M sulfuric acid with 1 mM Triton X-100 surfactant. Light from a Xe arc lamp was passed through an SP-50 monochromator (Acton Research) and focused onto the middle of the device in an “underfill” configuration to mitigate any uncertainty in active surface area. The monochro-

mated output was measured using a calibrated GaInP_2 (1.8 eV) photodiode that was grown and processed at NREL. During durability measurements, a 250 W quartz tungsten-halogen lamp with a light shaping diffuser (Newport) and a water-filled IR filter was used as the illumination source for its longer bulb lifetime and more stable power output. The electrolyte during durability measurements was 0.5 M H_2SO_4 , with no surfactant.

Physical Characterization. X-ray photoelectron spectroscopy (XPS) (PHI Versaprobe III) was used to probe the chemical composition and state of the surface species of all three electrode architectures pre-test and post-test. The C 1s peak was set to 284.8 eV to calibrate binding energy for all spectra. The following transitions were probed: Mo 3d, S 2p, Ga 2p_{3/2}, In 3d, P 2p, and Al 2p. Photoelectrode degradation was monitored by *in situ* optical microscopy (AM7915MZTL – EDGE, Dino-Lite).

■ ASSOCIATED CONTENT

Supporting Information

The Supporting Information is available free of charge at <https://pubs.acs.org/doi/10.1021/acsami.1c18938>.

Additional materials characterization (XPS and optical microscopy) and electrochemical characterization (chronoamperometry measurements on replicate samples and postdurability test LSVs) (PDF)

Movie S1: Time lapse movie of the $\text{MoS}_2/\text{GaInP}_2$ device surface during durability measurement. A frame was taken every 5 min, and the movie has 1 frame per 1 s (MP4)

Movie S2: Time lapse movie of the $\text{MoS}_2/\text{WL}/\text{GaInP}_2$ device surface during durability measurement. A frame was taken every 5 min, and the movie has 1 frame per 1 s (MP4)

Movie S3: Time lapse movie of the $\text{MoS}_2/\text{CL}/\text{WL}/\text{GaInP}_2$ device surface during durability measurement. A frame was taken every 5 min, and the movie has 1 frame per 1 s (MP4)

■ AUTHOR INFORMATION

Corresponding Authors

James L. Young – Chemistry and Nanoscience Center, National Renewable Energy Laboratory, Golden, Colorado 80401, United States; Email: james.young@nrel.gov

Thomas F. Jaramillo – Department of Chemical Engineering, Stanford University, Stanford, California 94305, United States; SUNCAT Center for Interface Science and Catalysis, Stanford University, Stanford, California 94305, United States; orcid.org/0000-0001-9900-0622; Email: jaramillo@stanford.edu

Authors

Micha Ben-Naim – Department of Chemical Engineering, Stanford University, Stanford, California 94305, United States; SUNCAT Center for Interface Science and Catalysis, Stanford University, Stanford, California 94305, United States; Present Address: Materials Science Division, Lawrence Livermore National Laboratory, Livermore, California 94551, United States; orcid.org/0000-0001-6087-7662

Chase W. Aldridge – Chemistry and Nanoscience Center, National Renewable Energy Laboratory, Golden, Colorado 80401, United States

Myles A. Steiner – Chemistry and Nanoscience Center, National Renewable Energy Laboratory, Golden, Colorado 80401, United States

Reuben J. Britto – Department of Chemical Engineering, Stanford University, Stanford, California 94305, United States; SUNCAT Center for Interface Science and Catalysis, Stanford University, Stanford, California 94305, United States

Adam C. Nielander – Department of Chemical Engineering, Stanford University, Stanford, California 94305, United States; SUNCAT Center for Interface Science and Catalysis, Stanford University, Stanford, California 94305, United States; orcid.org/0000-0002-3639-2427

Laurie A. King – Manchester Fuel Cell Innovation Centre, Manchester Metropolitan University, Manchester M1 5GD, United Kingdom; orcid.org/0000-0002-0772-2378

Todd G. Deutsch – Chemistry and Nanoscience Center, National Renewable Energy Laboratory, Golden, Colorado 80401, United States; orcid.org/0000-0001-6577-1226

Complete contact information is available at:
<https://pubs.acs.org/10.1021/acsami.1c18938>

Notes

The views expressed in the article do not necessarily represent the views of the DOE or the U.S. Government. The U.S. Government retains and the publisher, by accepting the article for publication, acknowledges that the U.S. Government retains a nonexclusive, paid-up, irrevocable, worldwide license to publish or reproduce the published form of this work, or allow others to do so, for U.S. Government purposes. The authors declare no competing financial interest.

ACKNOWLEDGMENTS

The authors gratefully acknowledge research support from the HydroGEN Advanced Water Splitting Materials Consortium, established as part of the Energy Materials Network under the U.S. Department of Energy, Office of Energy Efficiency and Renewable Energy, Hydrogen and Fuel Cell Technologies Office, under Award Number DE-EE-0008084. The authors thank Waldo Olavarria and Michelle Young for growth and processing work. This work was authored in part by the National Renewable Energy Laboratory, operated by Alliance for Sustainable Energy, LLC, for the U.S. Department of Energy under Contract Number DE-AC36-08GO28308. This work was performed under the auspices of the U.S. Department of Energy by Lawrence Livermore National Laboratory under Contract DE-AC52-07NA27344. Work was performed in part at the Stanford Nano Shared Facilities (SNSF) and the nano@ Stanford labs (SNF), which are supported by the National Science Foundation as part of the National Nanotechnology Coordinated Infrastructure under Award ECCS-2026822.

REFERENCES

- (1) Lewis, N. S.; Nocera, D. G. Powering the Planet: Chemical Challenges in Solar Energy Utilization. *Proc. Natl. Acad. Sci. U. S. A.* **2006**, *103*, 15729–15735.
- (2) Gray, H. B. Powering the Planet with Solar Fuel. *Nat. Chem.* **2009**, *1*, 7.
- (3) Ager, J. W.; Shaner, M. R.; Walczak, K. A.; Sharp, I. D.; Ardo, S. Experimental Demonstrations of Spontaneous, Solar-Driven Photoelectrochemical Water Splitting. *Energy Environ. Sci.* **2015**, *8*, 2811–2824.
- (4) McCrory, C. C. L.; Jung, S.; Ferrer, I. M.; Chatman, S. M.; Peters, J. C.; Jaramillo, T. F. Benchmarking Hydrogen Evolving

Reaction and Oxygen Evolving Reaction Electrocatalysts for Solar Water Splitting Devices. *J. Am. Chem. Soc.* **2015**, *137*, 4347–4357.

(5) McCrory, C. C. L.; Jung, S.; Peters, J. C.; Jaramillo, T. F. Benchmarking Heterogeneous Electrocatalysts for the Oxygen Evolution Reaction. *J. Am. Chem. Soc.* **2013**, *135*, 16977–16987.

(6) Seitz, L. C.; Chen, Z.; Forman, A. J.; Pinaud, B. A.; Benck, J. D.; Jaramillo, T. F. Modeling Practical Performance Limits of Photoelectrochemical Water Splitting Based on the Current State of Materials Research. *ChemSusChem* **2014**, *7*, 1372–1385.

(7) Khaselev, O.; Turner, J. A. A Monolithic Photovoltaic-Photoelectrochemical Device for Hydrogen Production via Water Splitting. *Science (80-)*. **1998**, *280*, 425–427.

(8) Verlage, E.; Hu, S.; Liu, R.; Jones, R. J. R.; Sun, K.; Xiang, C.; Lewis, N. S.; Atwater, H. A. A Monolithically Integrated, Intrinsically Safe, 10% Efficient, Solar-Driven Water-Splitting System Based on Active, Stable Earth-Abundant Electrocatalysts in Conjunction with Tandem III–V Light Absorbers Protected by Amorphous TiO₂ Films. *Energy Environ. Sci.* **2015**, *8*, 3166–3172.

(9) Steiner, M. A.; Barraugh, C. D.; Aldridge, C. W.; Alvarez, I. B.; Friedman, D. J.; Ekins-Daukes, N. J.; Deutsch, T. G.; Young, J. L. Photoelectrochemical Water Splitting Using Strain-Balanced Multiple Quantum Well Photovoltaic Cells. *Sustain. Energy Fuels* **2019**, *3*, 2837–2844.

(10) Young, J. L.; Steiner, M. A.; Döscher, H.; France, R. M.; Turner, J. A.; Deutsch, T. G. Direct Solar-to-Hydrogen Conversion via Inverted Metamorphic Multi-Junction Semiconductor Architectures. *Nat. Energy* **2017**, *2*, 17028.

(11) Cheng, W.-H.; Richter, M. H.; May, M. M.; Ohlmann, J.; Lackner, D.; Dimroth, F.; Hannappel, T.; Atwater, H. A.; Lewerenz, H.-J. Monolithic Photoelectrochemical Device for Direct Water Splitting with 19% Efficiency. *ACS Energy Lett.* **2018**, *3*, 1795–1800.

(12) Ben-Naim, M.; Britto, R. J.; Aldridge, C. W.; Mow, R.; Steiner, M. A.; Nielander, A. C.; King, L. A.; Friedman, D. J.; Deutsch, T. G.; Young, J. L.; Jaramillo, T. F. Addressing the Stability Gap in Photoelectrochemistry: Molybdenum Disulfide Protective Catalysts for Tandem III–V Unassisted Solar Water Splitting. *ACS Energy Lett.* **2020**, *5*, 2631–2640.

(13) *Fuel Cell Technologies Office Multi-Year Research, Development, and Demonstration Plan, 2015*; United States Department of Energy: Washington, D.C., 2015.

(14) Olson, J. M.; Kurtz, S. R.; Kibbler, A. E.; Faine, P. A. 27.3% Efficient Ga_{0.5}In_{0.5}P/GaAs Tandem Solar Cell. *Appl. Phys. Lett.* **1990**, *56*, 623–625.

(15) Willardson, R.; Nalwa, H. S. *Processing and Properties of Compound Semiconductors*; Academic Press: San Diego, 2001.

(16) Deutsch, T. G.; Steiner, M. A.; Friedman, D. J.; Young, J. L.; France, R. M.; Turner, J. A.; Döscher, H. Passivating Window and Capping Layer for Photoelectrochemical Cells. United States Patent US10,927,466B2, 2021.

(17) Hu, S.; Lewis, N. S.; Ager, J. W.; Yang, J.; McKone, J. R.; Strandwitz, N. C. Thin-Film Materials for the Protection of Semiconducting Photoelectrodes in Solar-Fuel Generators. *J. Phys. Chem. C* **2015**, *119*, 24201–24228.

(18) Montoya, J. H.; Seitz, L. C.; Chakhranont, P.; Vojvodic, A.; Jaramillo, T. F.; Nørskov, J. K. Materials for Solar Fuels and Chemicals. *Nat. Mater.* **2017**, *16*, 70–81.

(19) Chen, Z.; Cummins, D.; Reinecke, B. N.; Clark, E.; Sunkara, M. K.; Jaramillo, T. F. Core-Shell MoO₃-MoS₂ Nanowires for Hydrogen Evolution: A Functional Design for Electrocatalytic Materials. *Nano Lett.* **2011**, *11*, 4168–4175.

(20) Merki, D.; Fierro, S.; Vrabel, H.; Hu, X. Amorphous Molybdenum Sulfide Films as Catalysts for Electrochemical Hydrogen Production in Water. *Chem. Sci.* **2011**, *2*, 1262–1267.

(21) Britto, R. J.; Benck, J. D.; Young, J. L.; Hahn, C.; Deutsch, T. G.; Jaramillo, T. F. Molybdenum Disulfide as a Protection Layer and Catalyst for Gallium Indium Phosphide Solar Water Splitting Photocathodes. *J. Phys. Chem. Lett.* **2016**, *7*, 2044–2049.

(22) Britto, R. J.; Young, J. L.; Yang, Y.; Steiner, M. A.; LaFehr, D. T.; Friedman, D. J.; Beard, M. C.; Deutsch, T. G.; Jaramillo, T. F.

Interfacial Engineering of Gallium Indium Phosphide Photoelectrodes for Hydrogen Evolution with Precious Metal and Non-Precious Metal Based Catalysts. *J. Mater. Chem. A* **2019**, *7*, 16821–16832.

(23) King, L. A.; Hellstern, T. R.; Park, J.; Sinclair, R.; Jaramillo, T. F. Highly Stable Molybdenum Disulfide Protected Silicon Photocathodes for Photoelectrochemical Water Splitting. *ACS Appl. Mater. Interfaces* **2017**, *9*, 36792–36798.

(24) Benck, J. D.; Lee, S. C.; Fong, K. D.; Kibsgaard, J.; Sinclair, R.; Jaramillo, T. F. Designing Active and Stable Silicon Photocathodes for Solar Hydrogen Production Using Molybdenum Sulfide Nanomaterials. *Adv. Energy Mater.* **2014**, *4*, 1400739.

(25) Laursen, A. B.; Pedersen, T.; Malacrida, P.; Seger, B.; Hansen, O.; Vesborg, P. C. K.; Chorkendorff, I. MoS₂ - An Integrated Protective and Active Layer on n⁺p-Si for Solar H₂ Evolution. *Phys. Chem. Chem. Phys.* **2013**, *15*, 20000–20004.

(26) Lancaster, M.; Mow, R.; Liu, J.; Cheek, Q.; Macinnes, M. M.; Al-Jassim, M. M.; Deutsch, T. G.; Young, J. L.; Maldonado, S. Protection of GaInP₂ Photocathodes by Direct Photoelectrodeposition of MoS_x Thin Films. *ACS Appl. Mater. Interfaces* **2019**, *11*, 25115–25122.

(27) Gu, J.; Aguiar, J. A.; Ferrere, S.; Steirer, K. X.; Yan, Y.; Xiao, C.; Young, J. L.; Al-Jassim, M.; Neale, N. R.; Turner, J. A. A Graded Catalytic–Protective Layer for an Efficient and Stable Water-Splitting Photocathode. *Nat. Energy* **2017**, *2*, 16192.

(28) Fairley, N.; Fernandez, V.; Richard-Plouet, M.; Guillot-Deudon, C.; Walton, J.; Smith, E.; Flahaut, D.; Greiner, M.; Biesinger, M.; Tougaard, S.; Morgan, D.; Baltrusaitis, J. Systematic and Collaborative Approach to Problem Solving Using X-Ray Photoelectron Spectroscopy. *Appl. Surf. Sci. Adv.* **2021**, *5*, 100112.

(29) Young, J. L.; Steirer, K. X.; Dzara, M. J.; Turner, J. A.; Deutsch, T. G. Remarkable Stability of Unmodified GaAs Photocathodes during Hydrogen Evolution in Acidic Electrolyte. *J. Mater. Chem. A* **2016**, *4*, 2831–2836.

(30) Döscher, H.; Young, J. L.; Geisz, J. F.; Turner, J. A.; Deutsch, T. G. Solar-to-Hydrogen Efficiency: Shining Light on Photoelectrochemical Device Performance. *Energy Environ. Sci.* **2016**, *9*, 74–80.

(31) Chen, Z.; Jaramillo, T. F.; Deutsch, T. G.; Kleiman-Shwarsctein, A.; Forman, A. J.; Gaillard, N.; Garland, R.; Takanabe, K.; Heske, C.; Sunkara, M.; McFarland, E. W.; Domen, K.; Miller, E. L.; Turner, J. A.; Dinh, H. N. Accelerating Materials Development for Photoelectrochemical Hydrogen Production: Standards for Methods, Definitions, and Reporting Protocols. *J. Mater. Res.* **2010**, *25*, 3–16.

(32) Hwang, S.; Young, J. L.; Mow, R.; Laursen, A. B.; Li, M.; Yang, H.; Batson, P. E.; Greenblatt, M.; Steiner, M. A.; Friedman, D.; Deutsch, T. G.; Garfunkel, E.; Dismukes, G. C. Highly Efficient and Durable III–V Semiconductor-Catalyst Photocathodes via a Transparent Protection Layer. *Sustain. Energy Fuels* **2020**, *4*, 1437–1442.

(33) Pishgar, S.; Strain, J. M.; Gulati, S.; Sumanasekera, G.; Gupta, G.; Spurgeon, J. M. Investigation of the Photocorrosion of N-GaP Photoanodes in Acid with in Situ UV-Vis Spectroscopy. *J. Mater. Chem. A* **2019**, *7*, 25377–25388.

(34) Jain, N.; Schulte, K. L.; Geisz, J. F.; Friedman, D. J.; France, R. M.; Perl, E. E.; Norman, A. G.; Guthrey, H. L.; Steiner, M. A. High-Efficiency Inverted Metamorphic 1.7/1.1 EV GaInAsP/GaInAs Dual-Junction Solar Cells. *Appl. Phys. Lett.* **2018**, *112*, 053905.

NOTE ADDED AFTER ASAP PUBLICATION

This paper was published ASAP on January 10, 2022. A number of additional minor corrections were made and the corrected version was reposted on January 12, 2022.



ACS IN FOCUS

Cellular Agriculture
Lab-Grown
Dilek Erilliç
Dorothee E.

Machine Learning in Chemistry
Jon Paul Janet & Heather J. Kulik

bacterials
Lioria Cheng Jaramillo
William M. Wuest

ACS In Focus ebooks are digital publications that help readers of all levels accelerate their fundamental understanding of emerging topics and techniques from across the sciences.

pubs.acs.org/series/infocus

ACS Publications
Most Trusted. Most Cited. Most Read.

QR code